Vol. 71: 17–31, 2016
doi: 10.3354/cr01418

CLIMATE RESEARCH
Clim Res

Published online November 14

Global warming-induced changes in climate zones based on CMIP5 projections

Michal Belda*, Eva Holtanová, Jaroslava Kalvová, Tomáš Halenka

Charles University in Prague, Dept. of Meteorology and Environment Protection, 18200, Prague, Czech Republic

ABSTRACT: Climate classifications can provide an effective tool for integrated assessment of climate model results. We present an analysis of future global climate projections performed in the framework of the Coupled Model Intercomparison Project Phase 5 (CMIP5) project by means of Köppen-Trewartha classification. Maps of future climate type distributions were created along with the analysis of the ensemble spread. The simulations under scenarios with representative concentration pathway (RCP) 4.5 and RCP8.5 showed a substantial decline in ice cap, tundra, and boreal climate in the warming world, accompanied by an expansion of temperate climates, dry climates, and savanna, nearly unanimous within the CMIP5 ensemble. Results for the subtropical climate types were generally not conclusive. Changes in climate zones were also analyzed in comparison with the individual model performance for the historical period 1961–1990. The magnitude of change was higher than model errors only for tundra, boreal, and temperate continental climate types. For other types, the response was mostly smaller than model error, or there was considerable disagreement among the ensemble members. Altogether, around 14% of the continental area is expected to change climate types by the end of the 21st century under the projected RCP4.5 forcing and 20% under the RCP8.5 scenario.

KEY WORDS: Köppen-Trewartha climate classification · Coupled Model Intercomparison Project Phase 5 · CMIP5 · Global climate model · Climate type change · Representative concentration pathways

1. INTRODUCTION

The outputs of state-of-the-art global climate models are currently available within the Coupled Model Intercomparison Project Phase 5 (CMIP5, Taylor et al. 2012b), which served as the basis for the IPCC's Fifth Assessment Report, published in September 2013 (available online at www.ipcc.ch). Besides the global climate models (GCMs) themselves, which were improved, e.g. toward higher resolution and in some cases by including new processes and interactions such as so-called Earth System Models (ESMs), the methodology regarding the construction of projection scenarios also changed in comparison to previous GCM experiments (CMIP3 GCMs, Meehl et al. 2007). For the core CMIP5 GCM experiments, 4 representative concentration pathways (RCPs) with radiative forcing ranging from 2.6 to 8.5 W m^{-2} in the year 2100 were chosen, designated as RCP2.6, RCP4.5, RCP6.0, and RCP8.5 (Moss et al. 2010).

Each generation of climate models must inevitably be subject to tests of how realistic the models are in simulating the observed climate characteristics in the recent past. The climate classifications can serve, inter alia, as effective tools for analysis of model performance. The Köppen classification (Köppen 1923, 1931, 1936, Geiger 1954) or Köppen-Trewartha classification (KTC, Trewartha 1968, Trewartha & Horn 1980) have most often been used for this purpose. The climate types are based on long-term climatological means of near-surface air temperature and precipitation that are easily obtained from the outputs of GCMs. The KTC provides a slightly more detailed description of climate type distributions than the original

*Corresponding author: Michal.Belda@mff.cuni.cz

Publisher: Inter-Research · www.int-res.com

Köppen scheme (de Castro et al. 2007). Belda et al. (2014) reviewed the KTC and its differences from the original Köppen scheme, and analyzed observed patterns in climate types and their changes during the 20th century.

Climate types derived from GCM projections of future climate are useful for a variety of sectors and scientific fields. They provide an idea of what changes can be expected in the areas of individual climate types. Due to their strong relationship with the distribution of natural vegetation zones (e.g. Trewartha & Horn 1980, Bailey 2009), it is possible to assess the development of different ecoregions, even though further information on e.g. edaphic and topografic properties (Baker et al. 2010, Hargrove & Hoffman 2004) is needed for such assessments.

Projected changes in climate types have previously been analyzed in various studies using different climate models and emission scenarios. Lohmann et al. (1993) assessed the outputs of the atmospheric general circulation model ECHAM3 using the Köppen classification, and derived shifts in climate zones in greenhouse gas warming simulations over 100 model years. They projected a retreat of the permafrost climate and an extension of both the tropical rainy climate and dry climate.

Kalvová et al. (2003) applied the Köppen classification to simulations of 4 GCMs, namely HadCM2, ECHAM4, CSIRO-Mk2b, and CGCM1, for the present and future periods. They confirmed the results described by Lohmann et al. (1993) regarding tropical and dry climates and described a decline in the area of boreal and cold climates.

More recently, Rubel & Kottek (2010) created a series of digital world maps of Köppen climate types for the period 1901–2100 based on observed data (CRU TS2.1, GPCC Version 4) and 20 simulations of 5 GCMs (each GCM with 4 Special Report on Emission Scenarios [SRES] emission scenarios). In the case of the emission scenario with the highest rate of emission increase (A1FI), the results showed an increase in the areas covered by tropical, dry, and temperate climates, and a decrease in the coverage of cold and boreal climates. Projected changes for the milder emissions scenario (B1) were significantly smaller.

Baker et al. (2010) compared KTC types over China for historical (1961–1990) and projected future climates (2041–2070) simulated by HadCM3 for the SRES A1FI scenario. They showed that the spatial patterns of climate change resulted in a northern migration of warmer climatic types as well as a slight expansion in the high-latitude desert and arid shrubland regions in northwestern China.

Mahlstein et al. (2013) used simulations of 13 CMIP5 GCMs for determination of Köppen-Geiger climate types and analyzed their changes during 1900–2098. They found that under the RCP8.5 forcing, for which the mean warming reaches about 4.5°C by the end of the 21st century (Rogelj et al. 2012), approximately 20% of the global land area would undergo a shift in the original climate zones. Frost climates are projected to largely decline, some arid climatic zones are expected to expand, and large parts of the global land area with cool summers will experience a change to climates with hot summers. However, Mahlstein et al. (2013) also emphasized large model uncertainties and reported that the pace of the climate type shifts increases with increasing global mean temperature.

Feng et al. (2012) analyzed observed and projected climate changes and their impact on vegetation for the area north of 50° N over the period of 1900–2099 using the KTC scheme. To estimate the future changes, they used the simulations of 16 CMIP3 GCMs for 3 SRES emission scenarios (B1, A1B, and A2). Their results showed a decrease in areas classified as tundra, ice cap, and subarctic continental climates, and an expansion of the temperate and boreal oceanic climates. Moreover Feng et al. (2012) projected that arid, warm temperate, and snow and polar climates will successively shift to the north in the northern hemisphere.

Feng et al. (2014) focused on shifts in KTC climate types in 1900–2100. In contrast to Feng et al. (2012), the analysis was done for the whole global land area and model simulations of 20 CMIP5 GCMs for RCP4.5 and RCP8.5 pathways. Feng et al. (2014) found that during the 21st century, the KTC types would shift toward warmer and drier types, with the largest changes in the northern hemisphere north of 30° N. They also concluded that temperature changes are the dominant factor causing the projected shifts in climate types during the 21st century.

Here we used the KTC to assess changes in climate type areas simulated by a suite of 30 CMIP5 GCMs for the period of 2006–2100 and 2 RCPs (RCP4.5 and RCP8.5). Our study follows previous papers, i.e. Belda et al. (2014) mentioned above and Belda et al. (2015), wherein we assessed the performance of 43 CMIP5 GCMs in simulating the KTC climate types in the reference period 1961–1990. One of the main conclusions of Belda et al.'s (2015) analysis was that models generally had problems capturing the rainforest climate type *Ar* (see Table 2 for climate types), mainly in Amazonia. The desert climate type *BW* was underestimated by half of the models. Boreal climate

type *E* was overestimated by many models, mostly spreading over to the areas of observed tundra type *Ft*. Further, Belda et al. (2015) indicated that CMIP5 GCMs did not show any clear tendency to improve the representation of climate types with increasing spatial resolution.

In addition to previous analyses of CMIP5 models in terms of Köppen classification by Mahlstein et al. (2013) and Feng et al. (2014), here we use the largest possible set of GCMs, describe the temporal evolution of KTC types for individual GCMs, and present simulated changes in the context of model performance for the present climate. We also add an analysis of future climate uncertainty in terms of ensemble spread throughout the scenario simulations.

Various supplementary graphical products, including figures describing the model performance of CMIP5 GCMs used by Belda et al. (2015) are available at http://kfa.mff.cuni.cz/projects/trewartha/.

2. DATA AND METHODS

2.1. Data

A suite of CMIP5 GCM simulations is employed here, selected based on the availability of data for both RCP4.5 and RCP8.5 scenarios. Basic information on all model simulations incorporated here is presented in Table 1. The data are available at http://cmip-pcmdi.llnl.gov/cmip5/; we used monthly mean surface air temperature and precipitation to classify the KTC types. The outputs from the experiment denoted as 'historical' were used for the reference period 1961–1990. For the future time period 2006–2100, we considered 2 alternative simulations, RCP4.5 and RCP8.5. RCP4.5 assumes radiative forcing of 4.5 W m^{-2} at stabilization after 2100, whereas RCP8.5 represents a 'rising pathway' with radiative forcing higher than 8.5 W m^{-2} after 2100. For more details on RCPs, see Moss et al. (2010). Where more ensemble members were available, we chose the ensemble member r1i1p1 (considered a baseline simulation of the subensemble for the puposes of this analysis) (Taylor et al. 2012a).

As one of the indicators of uncertainty in the climate signal, errors in the historical experiment during the reference period were considered in terms of KTC types based on monthly mean surface air temperature and precipitation provided by the Climatic Research Unit (CRU) TS 3.22 dataset (Harris et al. 2014, hereafter TS3) available in spatial resolution of 0.5° × 0.5° over global land areas excluding Antarctica. As a part of the uncertainty analysis, a comparison of the classification based on 2 versions of CRU (TS 3.22 and TS 3.1.10) and the University of Delaware dataset version 4.01 (UDEL; Willmott & Matsuura 2001) was performed with the conclusion that the differences between these datasets are considerably smaller than the spread of the model simulations, and thus the impact of the choice of the observational dataset on GCM performance evaluation is negligible.

2.2. Methods

The KTC system (Trewartha & Horn 1980, Belda et al. 2014) has 6 main climate groups. Five of them (*A*, *C*, *D*, *E*, and *F*) are basic thermal zones. The sixth group, *B*, is the dry climatic zone that cuts across the other climate types, except for the polar climate *F*. Similarly to original Köppen classification scheme, the main climate types are determined according to long-term annual and monthly means of surface air temperature and precipitation amounts. The dryness threshold distinguishing group *B* is based on the definition by Patton (1962). A brief summary of climate types and subtypes is provided in Table 2.

The KTC climate types were calculated in the original model grids for the reference period 1961–1990 and for running 30 yr periods during the 21st century, beginning with 2006–2035 until 2071–2100 or 2070–2099 (as data for some of the model runs are only available until the year 2099). Land areas falling into each climate type/subtype were expressed in terms of relative areas, i.e. as a percentage of the whole global land area (excluding Antarctica). Simulated changes of KTC types for both RCP4.5 and RCP8.5 were assessed in several different ways. An overall picture of the multi-model ensemble evolution in time is provided as medians and 10th and 90th percentiles of changes of relative areas with respect to the values simulated for the reference period 1961–1990.

Further, we pay special attention to 3 selected time periods denoted as near future (2006–2035), mid-century (2020–2050), and far future (2071–2100 or 2070–2099 based on the simulation period). We demonstrate changes in selected climate type areas for each of these periods simulated by individual GCMs together with model errors in the reference period indicating the reliability of the climate change signal. All changes are expressed in percentage of area simulated by the respective GCMs in the reference period. The model errors are defined as differences in

Table 1. CMIP5 global climate models analyzed in this study with model versions explained (where applicable)

No.	CMIP5 model	Resolution	Modeling center/model versions
1	ACCESS1.3	1.88° × 1.24°	Commonwealth Scientific and Industrial Research Organisation (CSIRO) and Bureau of Meteorology, Australia
2	CanESM2	2.8° × 2.8°	Canadian Centre for Climate Modelling and Analysis
3	CCSM4	1.25° × 0.94°	National Center for Atmospheric Research
4	CESM1-BGC	1.25° × 0.94°	Community Earth System Model Contributors BGC: BioGeoChemistry CAM5: Community Atmospheric Model v5 FV2: Finite volume 2degree
5	CESM1-CAM5	1.25° × 0.94°	
6	CESM1-CAM5.1-FV2	2.50° × 1.88°	
7	CNRM-CM5	1.4° × 1.4°	Centre National de Recherches Météorologiques; Centre Européen de Recherche et Formation Avancées en Calcul Scientifique
8	CSIRO-Mk3.6.0	1.9° × 1.9°	CSIRO; Queensland Climate Change Centre of Excellence
9	FGOALS-g2	2.81° × 3.00°	LASG, Institute of Atmospheric Physics, Chinese Academy of Sciences and CESS,Tsinghua University
10	GFDL-CM3	2.5° × 2°	Geophysical Fluid Dynamics Laboratory
11	GFDL-ESM2G	2.5° × 2°	
12	GFDL-ESM2M	2.5° × 2°	
13	GISS-E2-H	2.5° × 2°	NASA Goddard Institute for Space Studies H: Hycom Ocean Model R: Russell Ocean Model CC: interactive terrestrial carbon cycle, ocean biogeochemistry
14	GISS-E2-H-CC	2.5° × 2°	
15	GISS-E2-R	2.5° × 2°	
16	GISS-E2-R-CC	2.5° × 2°	
17	HadGEM2-AO		Met Office Hadley Centre AO: aerosols, ocean & sea-ice CC: AO+terrestrial carbon cycle, ocean biogeochemistry ES: CC+chemistry
18	HadGEM2-CC	1.875° × 1.25°	
19	HadGEM2-ES	1.875° × 1.25°	
20	INM-CM4	2° × 1.5°	Institute for Numerical Mathematics
21	IPSL-CM5A-MR	2.5° × 1.3°	Institut Pierre-Simon Laplace MR: Medium resolution LR: Low resolution
22	IPSL-CM5B-LR	3.75° × 1.9°	
23	MIROC5	1.4° × 1.4°	Atmosphere and Ocean Research Institute (The University of Tokyo), National Institute for Environmental Studies, and Japan Agency for Marine-Earth Science and Technology
24	MIROC-ESM	2.8° × 2.8°	Japan Agency for Marine-Earth Science and Technology, Atmosphere and Ocean Research Institute (The University of Tokyo), and National Institute for Environmental Studies CHEM: added atmospheric chemistry
25	MIROC-ESM-CHEM	2.8° × 2.8°	
26	MPI-ESM-LR	1.9° × 1.9°	Max Planck Institute for Meteorology MR: Medium resolution LR: Low resolution
27	MPI-ESM-MR	1.9° × 1.9°	
28	MRI-CGCM3	1.125° × 1.125°	Meteorological Research Institute
29	NorESM1-M	2.5° × 1.9°	Norwegian Climate Centre M: intermediate resolution ME: M+carbon cycle
30	NorESM1-ME	2.5° × 1.9°	

Table 2. Definition of Köppen-Trewartha classification (KTC) climate types according to Trewartha & Horn (1980), with dryness threshold defined by Patton (1962). *Tmo*: long-term monthly mean air temperature; *Tcold* (*Twarm*): monthly mean air temperature of the coldest (warmest) month; *Pmean*: mean annual precipitation (cm); *Pdry*: mean precipitation of the driest summer month; *R*: Patton's precipitation threshold, defined as $R = 2.3T - 0.64Pw + 41$, where T is mean annual temperature (°C) and Pw is the percentage of annual precipitation occurring in winter

Type Subtype	Criteria Precipitation/temperature regime
A	*Tcold* > 18°C; *Pmean* > *R*
Ar	10 to 12 mo wet; 0 to 2 mo dry
Aw	Winter (low-sun period) dry; >2 mo dry
As	Summer (high-sun period) dry; rare in type *A* climates
B	*Pmean* < *R*
BS	*R*/2 < *Pmean* < *R*
BW	*Pmean* < *R*/2
C	*Tcold* < 18°C; 8 to 12 mo with *Tmo* > 10°C
Cs	Summer dry; at least 3 times as much precipitation in winter half-year as in summer half-year; *Pdry* < 3 cm; total annual precipitation < 89 cm
Cw	Winter dry; at least 10 times as much precipitation in summer half-year as in winter half-year
Cf	No dry season; difference between driest and wettest month less than required for *Cs* and *Cw*; *Pdry* > 3 cm
D	4 to 7 mo with *Tmo* > 10°C
Do	*Tcold* > 0°C
Dc	*Tcold* < 0°C
E	1 to 3 mo with *Tmo* > 10°C
F	All months with *Tmo* < 10°C
Ft	*Twarm* > 0°C
Fi	*Twarm* < 0°C

simulated and observed CRU TS3.22 areas expressed as a percentage of observed values.

For illustration of the geographical distribution of changes simulated for the far-future period, maps of projected distributions of KTC types are shown for both RCPs. Climate zones in the future period were calculated based on temperature and precipitation scenarios constructed using the delta method (Deque 2007). Ensemble mean values in the periods 2070–2099 and 1961–1990 were used to calculate deltas that were then added (multiplied) to the present climate state represented by the temperature (precipitation) from the CRU TS3.22 database. KTC was then applied, which provided spatial distributions of climate zones in the scenarios.

3. RESULTS

The geographical distribution of observed KTC types and its simulated changes are illustrated in Figs. 1–3. The climate change signal patterns are similar for both scenarios, with stronger manifestation under stronger forcing of RCP8.5. In the northern hemisphere, the most remarkable feature is the northward shift of the border between *Dc* and *E* types, with an increase in the area of *Dc* and shrinking of the *E* type. The shift of the southern border of *Dc* is not as evident; only in Europe, an eastward shift of the *Dc*–*Do* border is projected, inducing expansion of the *Do* area over western and central Europe. Further, a global feature is shrinking of the *Ft* area, not only in the high latitudes, but also in high-elevation regions of the Himalayas and the Andes. In South America, the *Ft* type is projected to dissapear by the end of the century under both RCPs. Another distinct pattern of change in South America is the expansion of the dry types *BW* and *BS*. In Africa and Australia, the GCMs project an increase in the *BW* area and shrinking of the *C* types. In southeastern Asia, our results suggest an expansion of the *Aw* type, which might be connected to increased strength of the Indian summer monsoon as documented e.g. by Menon et al. (2013).

The values of multi-model medians of simulated changes, 10th and 90th percentiles, and the range between them for the period 2071–2100 under both RCP4.5 and RCP8.5 forcings are summarized in Table 3.

The KTC climate types can be divided into 3 groups (decreasing area, increasing area and no conclusive change) based on the temporal behavior of simulated continental areas belonging to respective KTC types during the 21st century under the RCP4.5 and RCP8.5 forcing. The first group comprises boreal climate *E*, tundra *Ft*, and ice cap climate *Fi* that, according to the GCMs analyzed in our study, are expected to retreat. These 3 types occur at high latitudes or altitudes.

All GCMs simulate a decrease in the continental coverage (Antarctica not included in the analysis) of ice cap climate *Fi* (Fig. 4), which is clearly seen for the multi-model median (M-MED). Under the RCP4.5 forcing, the relative area of *Fi* decreases to 73% (Table 3) of the value simulated for the reference period 1961–1990. In the case of RCP8.5, the decrease is even stronger, as the *Fi* area decreases to 52% of its reference value. The decrease to less than 90% is already expected in the period 2006–2035 for both scenarios. The multi-model spread of simulated

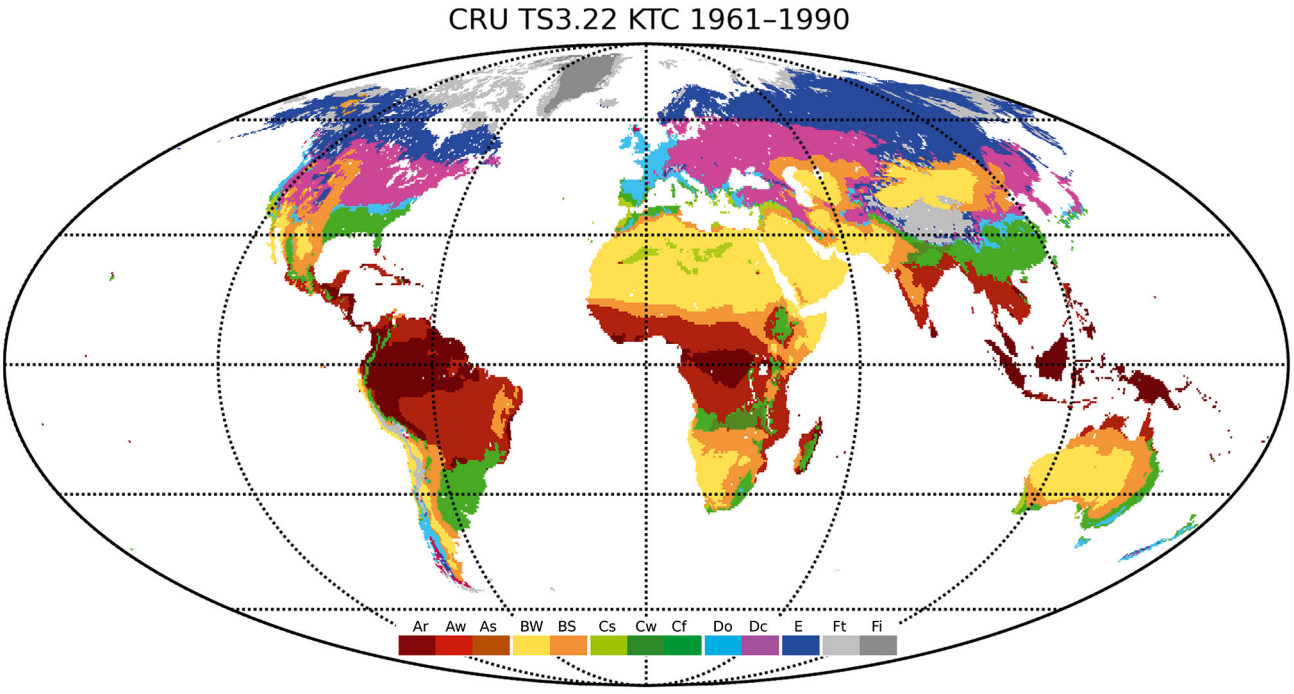

Fig. 1. Köppen-Trewartha climate types derived from observations (CRU TS3.22) for the period 1961–1990

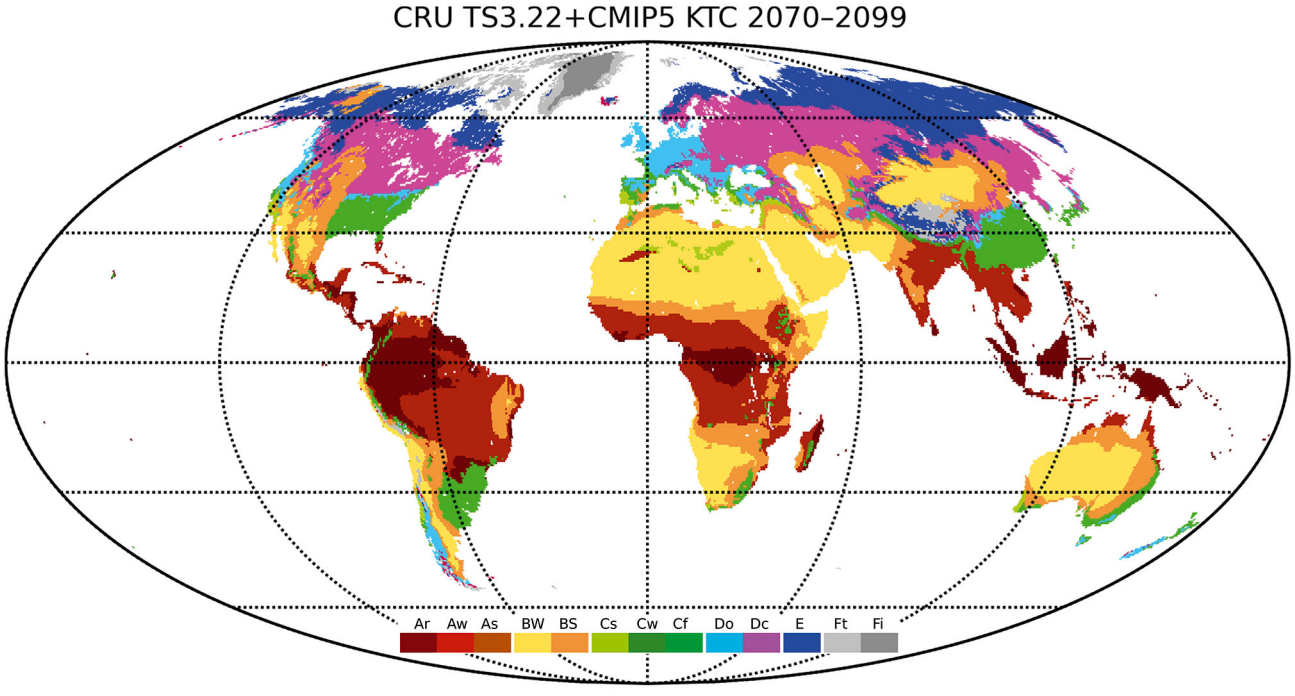

Fig. 2. Köppen-Trewartha climate types for the period 2070–2099, derived from the CRU TS3.22 observational dataset and the CMIP5 ensemble RCP4.5 scenario using the delta method

changes is quite large and is the same for both RCPs. In the case of RCP4.5, the decrease is often fastest during the first half of this century; in the second half it is rather slow, whereas the stronger forcing of RCP8.5 leads to more pronounced decline during the whole century. The decrease in relative area occupied by type *Fi* is solely due to transformation to tundra, *Ft*. Regarding the comparison of simulated changes to model errors in the reference period, all GCMs (except for CSIRO-Mk3-6-0 and MIROC-

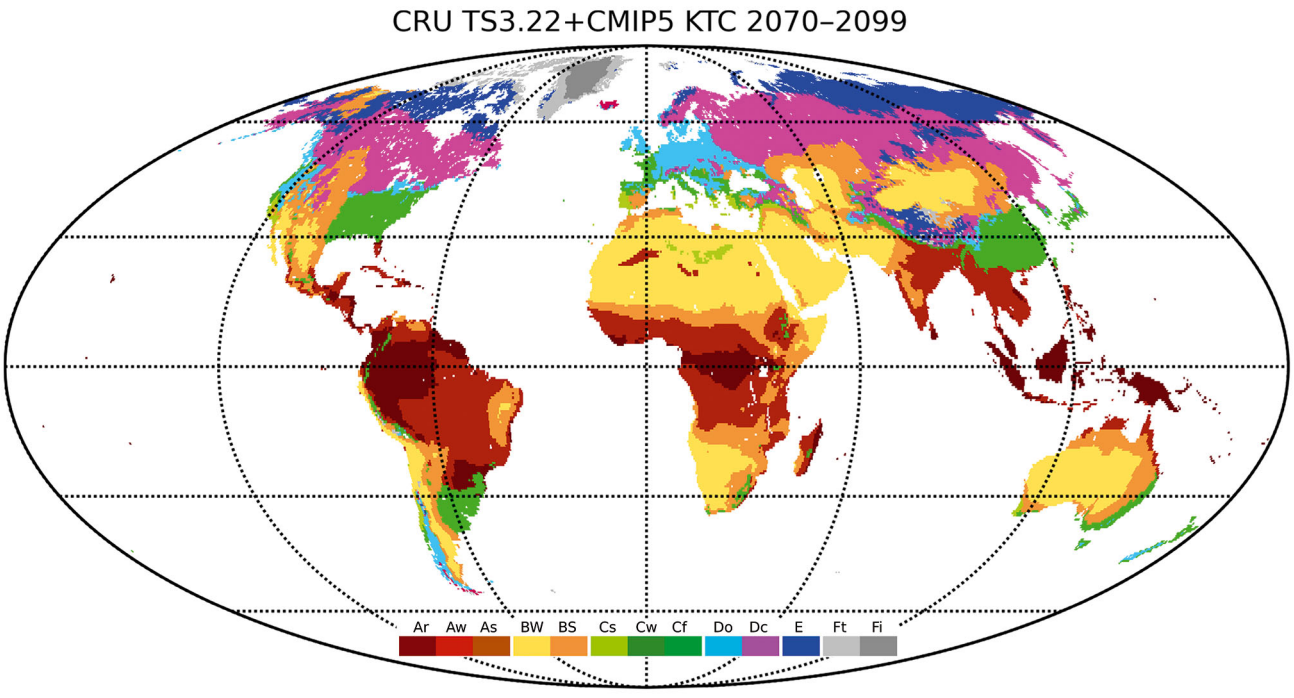

Fig. 3. Köppen-Trewartha climate types for the period 2070–2099, derived from the CRU TS3.22 observational dataset and the CMIP5 ensemble RCP8.5 scenario using the delta method

ESM) overestimate the observed area of *Fi*. Only in 37 out of 180 cases (3 periods, 2 RCPs, 30 GCMs) are the projected changes larger (in absolute value) than model errors (Fig. 5).

Similarly, all GCMs simulate a decrease in tundra climate type *Ft*, and under the RCP4.5 forcing, a faster rate of change occurs in the first half of the century (Fig. 4). According to M-MED, the relative area of *Ft* decreases by the end of the 21st century to 63% (42%) for RCP4.5 (RCP8.5), and the multi-model range is larger for RCP8.5 (Table 3). Models MIROC-ESM, MIROC-ESM-CHEM, and INMCM4 simulate the slowest decline in *Ft* (Fig. 5), even though the first 2 of these GCMs are the most sensitive to *Fi* changes. The largest change in *Ft* for the far future period is simulated by GFDL-CM3, which shows a decrease to 30% of the reference under RCP4.5 and 19% under RCP8.5. Projected changes are larger than model errors in 60% of all cases for RCP4.5, and in 90% for RCP8.5 at the end of the century. The *Ft* climate type is expected to transform into boreal climate *E*, although under RCP8.5, transitions of smaller areas to *Dc* and *Do* climate types are also simulated.

According to the outputs of all analyzed CMIP5 GCMs (except for GFDL-ESM2G and NorESM1-ME), the continental area occupied by boreal climate *E* is also expected to decrease (Fig. 5, Table 3). Time evolution of *E* type area in the running 30 yr periods according to individual GCMs shows a gradual monotonic decrease or only small fluctuations (Fig. 4). The exception is model CESM1-CAM5-1-FV2, which for both RCPs shows a negative peak around the year 2061 preceded by a steep decrease after 2045 and fol-

Table 3. Multi-model statistics of the percentage changes of Köppen-Trewartha classification (KTC; see Table 2 for definitions) climate type areas in the future with respect to the reference period (1961–1990) for the RCP4.5 and RCP8.5 scenarios. M-MED: multi-model median, p10: 10th percentile, p90: 90th percentile, range: range between p10 and p90

KTC	RCP4.5				RCP8.5			
type	M-MED	p10	p90	Range	M-MED	p10	p90	Range
Fi	73	57	85	28	52	40	68	28
Ft	63	45	77	32	42	28	66	38
E	83	67	97	30	64	36	86	50
Dc	115	106	127	21	130	116	145	29
Do	112	96	122	26	115	100	134	34
BW	108	103	117	14	113	108	123	15
BS	108	100	120	20	113	101	131	30
Aw	117	100	125	25	120	101	137	36
Ar	103	96	109	13	103	89	116	27
Cf	95	85	100	15	98	80	106	26
Cw	41	7	79	72	20	7	59	52
Cs	122	77	156	79	121	52	214	162

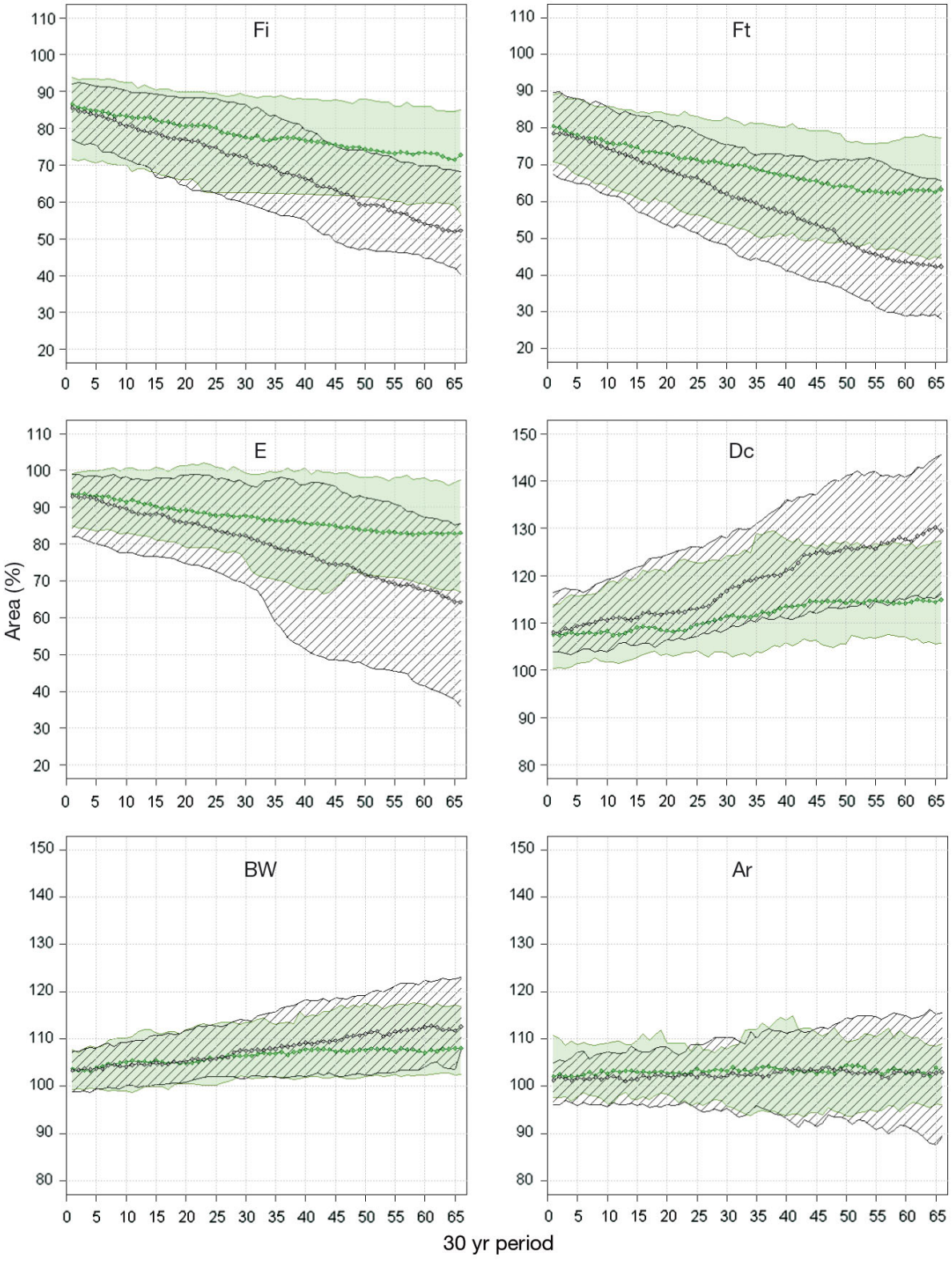

Fig. 4. Temporal evolution of continental area belonging to selected climate types (*Fi*, *Ft*, *E*, *Dc*, *BW*, and *Ar*; see Table 2 for definitions) for moving 30 yr periods throughout the 21st century relative to the reference period 1961–1990 (100% means no change); *x*-axis: 30 yr periods (period 1 is 2006–2035, period 66 is 2071–2100); squares: multi-model medians calculated from the ensemble of 30 selected CMIP5 GCMs (green for RCP4.5, black for RCP4.5); green area (diagonal hatching): values between the 10th and 90th percentiles of the multi-model ensemble for RCP4.5 (RCP8.5)

lowed by a steep rise until 2073 and a moderate decrease afterwards (not shown). This pattern both affects the spread of the results and is reflected in some other types (*Do*, *Dc, Ar*). Even though all GCMs simulated the observed area of type *E* with the smallest errors, their reactions to radiative forcing are quite diverse. The spread of the multi-model ensemble is larger for the stronger forcing of RCP8.5 than for RCP4.5 (Table 3). The decrease in continental area for type *E* by the end of the century seems to be the most convincing (in comparison to model errors, Fig. 5) of all climate types that are expected to decrease. Boreal climate transforms mainly to temperate continental climate *Dc*. For RCP8.5 the losses, generally from the southern extent of type E in the northern hemisphere, are >4 times larger than the gains of the area from tundra climate *Ft.*

The second group of KTC types consists of *Dc*, *Do*, *BW*, *BS*, and *Aw* that are all expected to increase their relative continental areas, according to most of the GCMs and both RCPs. All GCMs considered in our study (except for CESM1-CAM5-1-FV2) give a gradual expansion of continental temperate climate *Dc* during 2006–2100. Based on M-MED, the relative area occupied by *Dc* for RCP4.5 (RCP8.5) increases to approx. 115% (130%) of the area in the reference period by the end of the century (Fig. 5, Table 3). The stronger forcing of RCP8.5 leads to a higher increase in *Dc* area but also to a somewhat larger multi-model spread (Fig. 4, Table 3). Regarding the model errors, the GCMs tend to overestimate the observed area of *Dc*, but the errors are generally smaller in comparison to other KTC types. In the far-future period under RCP8.5, most of the simulated changes are larger than corresponding model errors (Fig. 5). The expansion of *Dc* is given mainly by the transition from *E*; for RCP8.5, a small portion also comes from *Ft*.

The expected increase in dry climate types *BW* and *BS* is not as convincing and well-marked as the increase in type *Dc*. According to M-MED, the relative continental area of desert climate *BW* grows by the end of the century to ~108% (113%) for RCP4.5 (RCP8.5) (Fig. 4, Table 3). Some of the GCMs, e.g. FGOALS-g2 and MRI-CGCM3, give a similar relative continental area for *BW* at the end of the 21st century as in the reference period (Fig. 5). The patterns in temporal behavior differ considerably among GCMs. Some models simulate a steady rise in *BW* area, others project a slight decrease during first decades followed by an increase or an increase followed by a short decline and a final rise. However, the multi-model spread of changes simulated for the end of the 21st century is one of the lowest of all KTC types. Both the simulated increase and the multi-model spread are larger for the RCP8.5 scenario. The simulated changes are larger than model errors for 50% (30%) of the GCMs for RCP8.5 (RCP4.5) in 2071–2100. Regarding the transitions between climate types, the *BW* gains the area mainly from *BS*. However, a small part of the *BW* area transforms into *BS*.

Our findings for steppe climate type *BS* are similar to *BW*. Most of the GCMs simulate a larger or similar relative continental area for *BS* at the end of the century with respect to the reference period (see Fig. S15 in the Supplement at www.int-res.com/articles/suppl/c071p017_supp.pdf). The multi-model median of changes represents an increase to 108% (113%) for RCP4.5 (RCP8.5) (Fig. S3, Table 3). For about half of the GCMs, under RCP8.5 in the far future, the expected change is greater than the model error. The expected climate changes lead to transition of *Cf* and *Aw* into *BS* and from *BS* into *BW*.

For savanna climate type *Aw*, most GCMs project a moderate expansion with M-MED of 117% (120%) for RCP4.5 (RCP8.5) (Fig. S2, Table 3). An exception is the model CanESM2, which projects a slight decrease in *Aw* area. Model errors are smaller than simulated changes for 2071–2100 according to 30% (50%) of simulations under RCP4.5 (RCP8.5). Similar to the case of boreal climate *E*, even though model performance in simulating *Aw* in the reference period is relatively good, the reactions to radiative forcing differ considerably among models. Part of the continental area occupied by *Aw* undergoes a transition to *BS* and a part of *Cf* area transforms into *Aw*.

Expected temporal evolution of relative continental area occupied by oceanic temperate climate *Do* differs between individual GCMs. Some of them project an increase in the area, others project an initial decrease and then a slow rise to approximately the same *Do* extent as simulated for the reference period. The time development of the 10th percentile (Fig. S8) shows that some GCMs even project a decrease in *Do* area in the far future, especially for RCP4.5. M-MED shows an overall change to 112% of the reference area for RCP4.5 and 115% for RCP8.5. Simulated changes in *Do* are smaller than model errors (Fig. S20), except for IPSL-CM5A-MR and HadGEM2-AO. Regarding the transitions between climate types, *Do* is expected to transform mainly into *Cf*.

Until now we have dealt with KTC types that are expected to decline or increase their area according to most CMIP5 GCMs, even though the sensitivity of the models was different and multi-model spread was quite large in some cases. Results for the remaining KTC types are less conclusive. Regarding the tropical

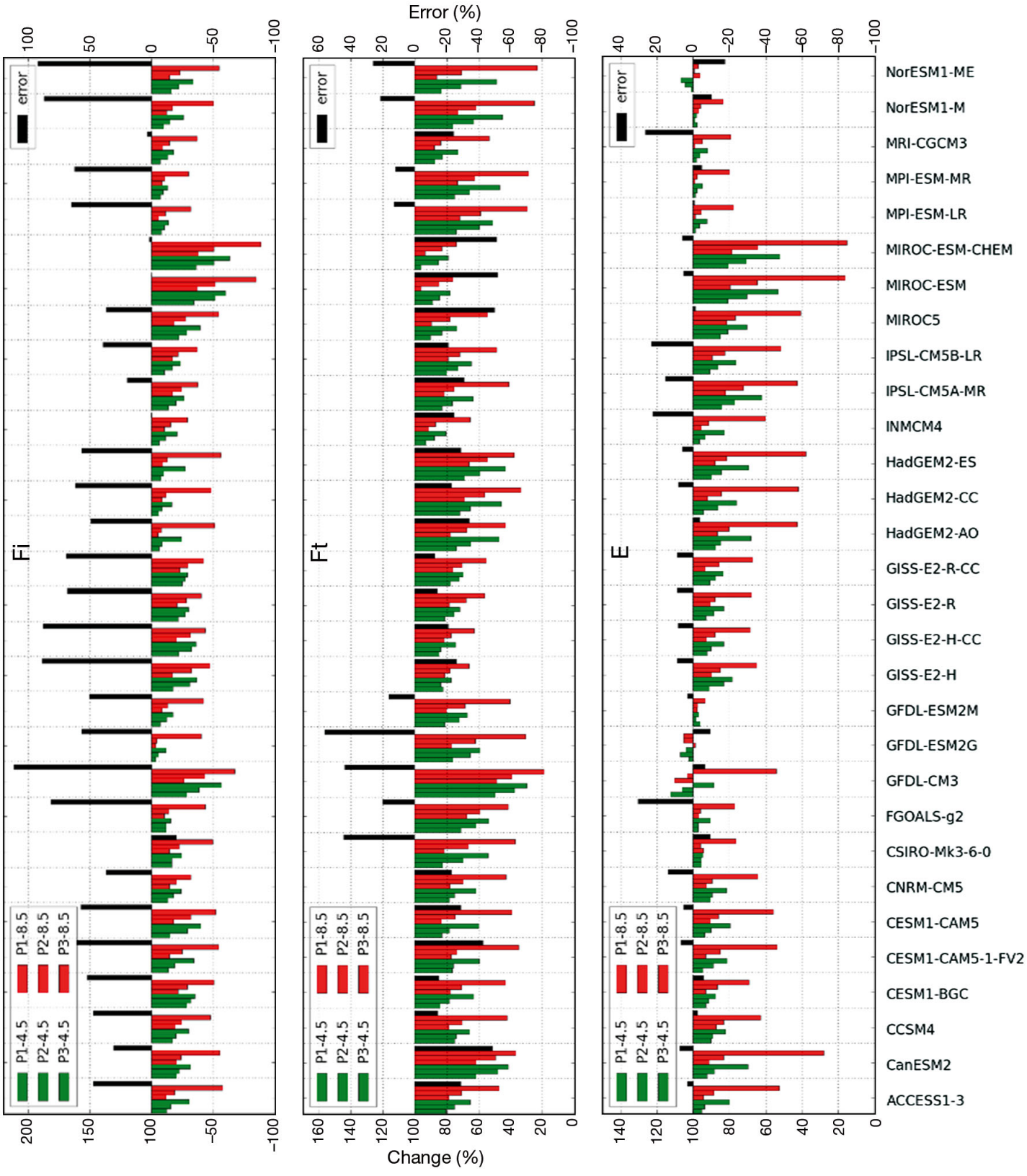

Fig. 5. Changes in relative continental areas of selected Köppen-Trewartha classification (KTC) climate types (*Fi, Ft, E, Dc, BW, Ar*; see Table 2 for definitions) projected for the periods 2006–2035 (P1), 2021–2050 (P2), and 2071–2100 (P3) relative to the reference period 1961–1990 (100% means no change) based on the ensemble of 30 selected CMIP5 GCMs for RCP4.5 (green) and RCP8.5 (red); error: model error in the reference period expressed as the difference between simulated and observed (based on CRU TS3.22) relative area in the percentage of the observed value

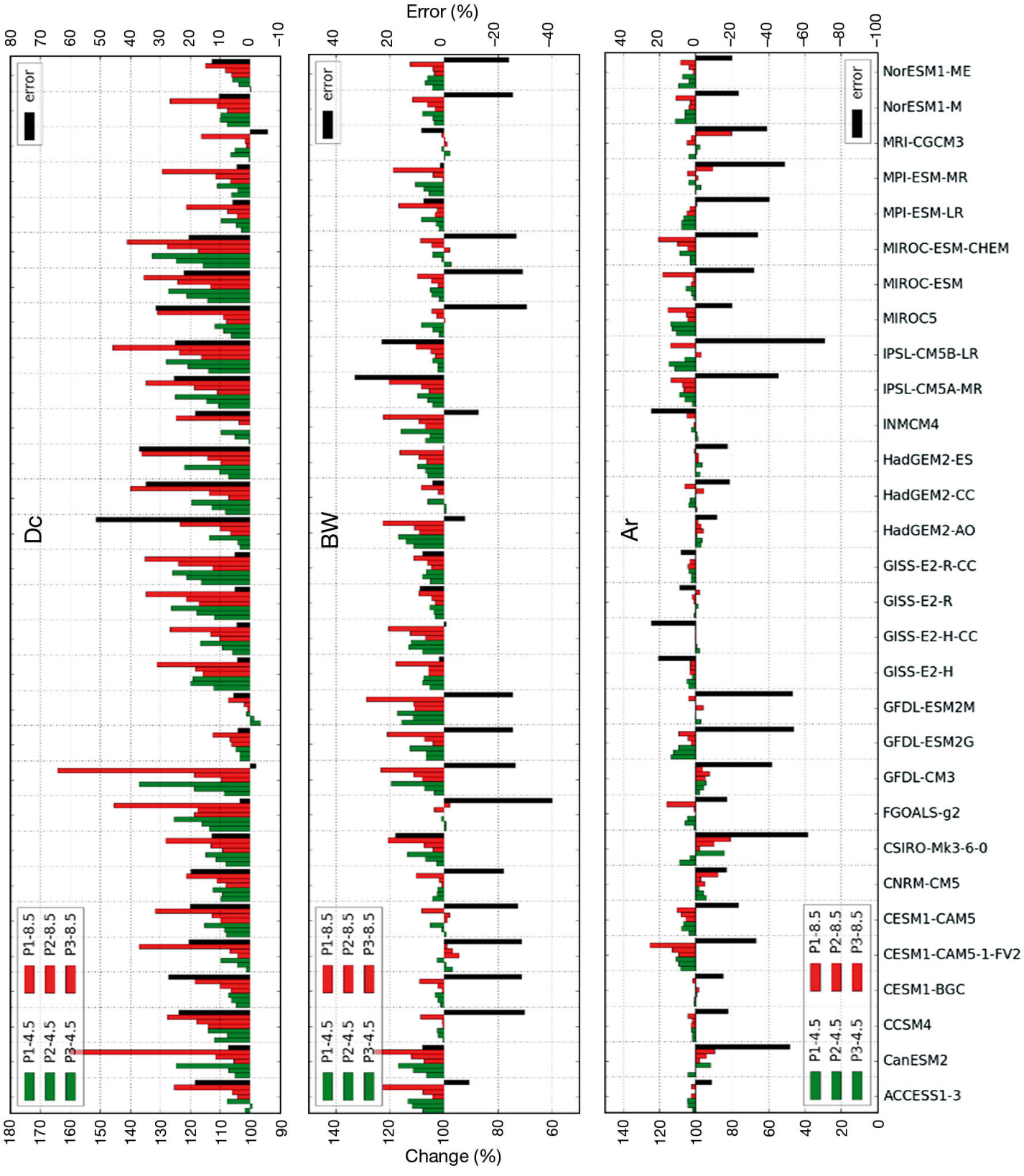

Fig. 5. (continued)

rainforest climate *Ar*, the ensemble does not show any significant signal, with ambiguous signs of change for individual GCM simulations (Fig. 5, Table 3). For both RCPs, the spread is rather small, similar to *BW* and *Cf*. The model errors are larger than simulated changes for all GCMs. The changes of *Ar* are given by transitions from *Aw* and *Cf* and into *Aw*.

Most of the GCMs simulate a decline in the area occupied by the subtropical humid climate *Cf* in 2006–2035, to ca. 95% of reference value according to M-MED. Thereafter, M-MED does not vary considerably, even though the multi-model spread grows throughout the century (Fig. S5). Simulated changes are mostly smaller than model errors, except for GISS-E2-R, GISS-E2-R-CC, and CanESM2 (Fig. S17). The subtropical humid climate *Cf* transforms mainly to *Aw* and *BS*. The area of type *Cf* increases due to gains from *Do*, *Dc*, and *BS*.

We do not discuss the results for *Cw* and *Cs*, as they both occupy a small fraction of global land area, and the spread of the model results is quite large. Therefore, it is difficult to draw any conclusions about their projected changes.

Overall, the GISS models and MRI-CGCM3, ACCESS1-3, GFDL-ESM2M, and NorESM1 have the least pronounced response to radiative forcing. For RCP8.5, these models simulate changes of ca. 16% of continental area (not including Antarctica). On the other hand, MIROC-ESM, MIROC-ESM-CHEM, GFDL-CM3, and CanESM2 show the largest KTC type changes. According to these GCMs, more than 30% of the considered land area will undergo a change of KTC type by the end of the 21st century. However, for individual KTC types, the models simulating the largest or smallest changes differ. For example, MIROC-ESM and MIROC-ESM-CHEM show the largest reduction in *Fi* but the slowest decline of *Ft*. It is noteworthy that GCMs developed in the same modeling center do not necessarily yield similar results. For example, GFDL-CM3 shows the most sensitive response of *Dc* area to radiative forcing, whereas GFDL-ESM2M gives a change of only 1% (7%) for RCP4.5 (RCP8.5) at the end of the century.

4. DISCUSSION AND CONCLUSIONS

We assessed changes in the global distributions of Köppen-Trewartha climate types throughout the 21st century as simulated by a suite of 30 CMIP5 global climate models for 2 representative concentration pathways, RCP4.5 and RCP8.5. Ice cap climate *Fi*, tundra *Ft*, and boreal climate *E* are expected to decline (Fig. 4). On the other hand, the relative continental area occupied by temperate climates *Dc* and *Do*, dry climates *BW* and *BS*, and savanna climate *Aw* will increase (with a few exceptions). The results for 2 remaining climate types, *Ar* and *Cf*, are less convincing; the changes are rather small, and the models do not even agree on the sign of the changes. Nevertheless, most of the GCMs simulate a slight decrease or increase at the beginning of the 21st century and very small changes thereafter. The types *Cs* and *Cw* cover only a small portion of the total continental area, and simulated changes have a large spread; therefore we will not discuss these types in detail.

Our conclusions about a decrease in *Fi* and *Ft* area and an increase in *Dc* and *Do* extent are consistent with the expected rise in near-surface air temperature and are in agreement with results described by other recent studies based on CMIP5 GCMs, e.g. by Feng et al. (2014), and also by studies for the previous generation of GCMs, e.g. Rubel & Kottek (2010).

Regarding the temporal evolution of relative continental areas covered by specific KTC types during the 21st century based on M-MED of simulated changes, a distinct difference in comparison to the reference period is already apparent for the first 30 yr time window of 2006–2035, and in most cases (except for *Ar* and *Cf*), the magnitude of simulated changes increases throughout the century. This pattern is more pronounced for RCP8.5. The course of simulated changes is not always smooth; for example, under RCP4.5 forcing, the decrease in area covered by *Ft* is faster during the first half of the century, while for RCP8.5 the decline is more stable. Similarly, under RCP4.5, the rate of increase/decrease of *BW*, *Dc*, and *Ar* is slower in the last third of the century. This might be partly due to differences in the RCPs; RCP4.5 represents a stabilization scenario with radiative forcing reaching its maximum in the second half of the 21st century; in contrast, under RCP8.5, radiative forcing increases throughout the whole 21st century (IPCC 2013). However, the influence of RCPs cannot be simply generalized. For example, the expansion of *Do* shows almost the same rate under both RCPs.

Considering the projections given by individual GCMs, for some KTC types the GCMs agree on the sign and general pattern of changes; however, the sensitivity of models to the radiative forcing differs for different KTC types (Fig. 5). For example, the models MIROC-ESM and MIROC-ESM-CHEM give the smallest change in *Ft* and the largest change in *Fi* (Fig. S24). The course of simulated changes is quite

smooth for some of the GCMs, while for others it exhibits wave-like behavior, breaks, and jumps even when using 30 yr running means.

The magnitude of changes for 3 selected time periods (near future, mid-century, far future) were compared to model errors in the reference period 1961–1990 (Fig. 5). The errors were evaluated from comparison of relative land areas of KTC types derived from GCM simulations and from CRU TS3.22 observations; in this way, they could be interpreted as biases as well. Regarding the end of the 21st century (far future), only for 3 out of 12 KTC types, viz. *Ft*, *E*, and *Dc,* the changes are higher than the model errors (according to most of GCMs under RCP8.5; under RCP4.5, half of the GCMs show that changes are higher than errors for *Dc*, and ca. 75% of GCMs indicate that this is the case for *E* and *Ft*). Thus, considering the model errors, the simulated decrease in relative continental area is clearly pronounced in the case of boreal climate *E* and tundra climate *Ft*, and the increase is pronounced in the case of continental temperate climate *Dc*. Regarding the expected decrease in *Fi* area, the simulated changes are larger than model errors according to only one-third of the GCMs for both RCP 8.5 and RCP 4.5. Further, in case of savanna climate *Aw*, dry climates *BW*, and steppe climate *BS*, the simulated changes in the far future are larger than model errors according to about half of the GCMs for both RCPs, except for dry climate *BW* under RCP4.5 (one-third of the models) and steppe climate *BS* under the same scenario (only 13%).

For *Cf* and *Do*, the simulated changes are larger than model errors according to only 6 and 4 out of 30 GCMs, respectively. The type *Ar* is the only KTC type for which the simulated changes are smaller than model errors for both RCPs and all 3 time periods. We found no straightforward relationship between the model performance and the strength of the climate signal in projected changes.

Besides a comparison of simulated changes to model errors, we assessed the uncertainty stemming from necessary choices in GCM structure. We used the range between the 10th and 90th percentile of the multi-model ensemble to assess this uncertainty. The smallest multi-model spread of simulated changes is seen for the *BW* type (Table 3), the largest for *E* and *Ft*. The simulated changes of *Ar*, *Cf*, and *Do* types are ambiguous in the sense that the multi-model ranges include a 'zero change'.

Considering the changes in relative areas for the KTC types all together, the lowest sensitivity to radiative forcing under RCP4.5 is seen for MRI-CGCM3, with 8% of total continental area undergoing a KTC type change until the end of the 21st century. Then follows a group of models with simulated changes of <12% (3 GISS GCMs, Nor-ESM1-M, Nor-ESM1-ME, GFDL-ESM2M, ACCESS1-3). For RCP8.5, the lowest sensitivity was found for all GISS models and MRI-CGCM3, with changes of 16–17%. The largest sensitivity was found for MIROC-ESM and MIROC-ESM-CHEM, with nearly a quarter of the global continental area (without Antarctica) showing changed KTC types under RCP4.5 and about 35% under RCP8.5. According to M-MED for RCP4.5 (RCP8.5), 14% (22%) of the continental area is expected to change its climate type by the end of the century. Our results are in agreement with Mahlstein et al. (2013), who projected that approximately 20% of global land will experience a change in climate type until 2100 under RCP8.5 forcing, although their study was based on a smaller number of models than ours. According to Feng et al. (2014), a larger portion of the continental area is expected to undergo a change in climate type (31% for RCP 4.5 and 46% for RCP8.5).

Regarding the shifts in the 6 major climate types, the changes projected for the far-future period under RCP8.5 based on our results and the study of Feng et al. (2014) are summarized in Table 4. The values are shown as a percentage of the respective KTC type area in the reference period 1961–1990. The simulated changes are more distinct for types *D*, *E*, and *F* than for other KTC types. For these 3 types, 25–50% of the reference area is expected to shift to another KTC type. This likely points to a more important influence of air temperature changes than precipitation changes on the KTC type shifts, which was shown by Feng et al. (2014) and Mahlstein et al. (2013).

Table 4. Comparison of multi-model statistics aggregated for the main Köppen-Trewartha classification (KTC) climate types (*A*–*F*, see Table 2 for definitions) in this study (rows 1–5) and in Feng et al. (2014, rows 6–9). Values are given as a percentage of the respective KTC type area in the reference period 1961–1990. M-MED: multi-model median, M-mean: multi-model mean, SD: standard deviation, F: Feng et al. (2014) values

		A	*B*	*C*	*D*	*E*	*F*
1	M-MED	17.4	13.2	−11.2	24.7	−37.4	−50.0
2	M-mean	14.9	15.6	−13.5	26.3	−39.4	−61.0
3	SD	10.1	6.3	12.7	9.3	22.3	27.4
4	M-mean – SD	4.9	9.3	−26.2	17.0	−61.7	−88.5
5	M-mean + SD	25.0	21.9	−0.8	35.5	−17.1	−33.6
6	Fmean	11.6	15.9	−13.4	40.0	−50.4	−59.2
7	FSD	4.0	5.3	7.9	13.7	16.9	10.8
8	Fmean – FSD	7.6	10.6	−21.3	26.3	−67.3	−70.0
9	Fmean + FSD	15.6	21.2	−5.5	53.7	−33.5	−48.4

For the purpose of comparing our results to the study of Feng et al. (2014), the multi-model mean (M-mean) and standard deviation (SD) were calculated for the 6 main climate types (Table 4). M-mean differs from M-MED most prominently for the *F* climate type, for which the SD has also the highest value. The values of M-mean according to our results and Feng et al. (2014) are fairly similar except for *D* and *E*, where Feng et al. (2014) found larger changes than presented in our analysis. The SD values according to Feng et al. (2014) are all smaller than our SD values, except for type *D*. In our study, we prefer the median and range between the 10th and 90th percentile to characterize the distribution of the multi-model ensemble, as the distribution of simulated KTC type changes is generally not symmetrical.

There are several possible reasons for the differences between our results and the results of Feng et al. (2014). The analyses are based on different groups of GCMs which may significantly influence the results, as individual models show different changes in KTC types in reaction to a given forcing. Further, we used model outputs in the original model grids, but Feng et al. (2014) applied a downscaling procedure to the GCM outputs. The fact that we investigated all continental areas excluding Antarctica, whereas Feng et al. (2014) only considered global continents north of 60° S, and the different observational datasets used could also play a role, although, as discussed previously, the differences are very small compared to the ensemble spread.

A change in relative continental areas of climate types is not the only expected impact of climate change. Potential geographical shifts are also very important. Our results indicate a poleward shift of *Ft*, *E*, *Do*, *Dc*, and *Cf* types (not shown). On the other hand, *Ar* and *Aw* types, which are found near the equator, did not experience any latitudinal shift. Regarding the dry climates, the GCMs do not agree entirely, especially in the case of *BW*. A detailed analysis of these shifts, however, is beyond the scope of this study and will be the subject of future investigations.

Acknowledgement. We acknowledge the World Climate Research Programme's Working Group on Coupled Modelling, which is responsible for CMIP, and we thank the climate modeling groups for producing and making available their model outputs. For CMIP the US Department of Energy's Program for Climate Model Diagnosis and Intercomparison provides coordinating support and led development of software infrastructure in partnership with the Global Organization for Earth System Science Portals. The CRU TS 3.22 dataset was provided by the Climatic Research Unit, University of East Anglia. This study was supported by project UNCE 204020/2012, funded by Charles University in Prague, and by research plan no. MSM0021620860 funded by the Ministry of Education, Youth and Sports of the Czech Republic. In addition, the work is part of the activity under the Program of Charles University PRVOUK No. 02 'Environmental Research'.

LITERATURE CITED

Bailey RG (2009) Ecosystem geography: from ecoregions to sites, 2nd edn. Springer, New York, NY

Baker B, Diaz H, Hargrove W, Hoffman F (2010) Use of the Köppen-Trewartha climate classification to evaluate climatic refugia in statistically derived ecoregions for the People's Republic of China. Clim Change 98:113–131

Belda M, Holtanová E, Halenka T, Kalvová J (2014) Climate classification revisited: from Köppen to Trewartha. Clim Res 59:1–13

Belda M, Holtanová E, Halenka T, Kalvová J, Hálvka Z (2015) Evaluation of CMIP5 present climate simulations using the Köppen-Trewartha climate classification. Clim Res 64:201–212

de Castro M, Gallardo C, Jylha K, Tuomenvirta H (2007) The use of a climate-type classification for assessing climate change effects in Europe from an ensemble of nine regional climate models. Clim Change 81:329–341

Deque M (2007) Frequency of precipitation and temperature extremes over France in an anthropogenic scenario: model results and statistical correction according to observed values. Global Planet Change 57:16–26

Feng S, Ho CH, Hu Q, Oglesby RJ, Jeong SJ, Kim BM (2012) Evaluating observed and projected future climate changes for the Artic using the Köppen–Trewartha climate classification. Clim Dyn 38:1359–1373

Feng S, Hu Q, Huang W, Ho CH, Li R, Tang Z (2014) Projected climate regime shift under future global warming from multi-model, multi-scenario CMIP5 simulation. Global Planet Change 112:41–52

Geiger R (1954) Klassifikationen der Klimate nach W. Köppen. In: Bartels J, ten Bruggencate P (eds) Landolt-Börnstein: Zahlenwerte und Funktionen aus Physik, Chemie, Astronomie, Geophysik und Technik (alte Serie), Vol 3. Springer, Berlin, p 603–607

Hargrove WW, Hoffman FM (2004) Potential of multivariate quantitative methods for delineation and visualization of ecoregions. Environ Manag 34:S39–S60

Harris I, Jones PD, Osborn TJ, Lister DH (2014) Updated high-resolution grids of monthly climatic observations — the CRU TS3.10 dataset. Int J Climatol 34:623–642

IPCC (Intergovernmental Panel on Climate Change) (2013) Climate Change 2013: the physical science basis. Cambridge University Press, Cambridge

Kalvová J, Halenka T, Bezpalcová K, Nemešová I (2003) Köppen climate types in observed and simulated climates. Stud Geophys Geod 47:185–202

Köppen W (1923) Die Klimate der Erde. Grundriss der Klimakunde. Walter de Gruyter & Co., Berlin

Köppen W (1931) Grundriss der Klimakunde. Walter de Gruyter & Co., Berlin

Köppen W (1936) Das geographische System der Klimate. In: Köppen W, Geiger R (eds) Handbuch der Klimatologie. Gebrüder Borntraeger, Berlin, p C1–C44

Lohmann U, Sausen R, Bengtsson L, Cubasch U, Perlwitz J,

Roeckner E (1993) The Köppen climate classification as a diagnostic tool for general circulation models. Clim Res 3:177–193

Mahlstein I, Daniel JS, Solomon S (2013) Pace of shifts in climate regions increases with global temperature. Nat Clim Change 3:739–743

Meehl GA, Covey C, Delworth T, Latif M and others (2007) The WCRP CMIP3 multi-model dataset: a new era in climate change research. Bull Am Meteorol Soc 88: 1383–1394

Menon A, Levermann A, Schewe J, Lehmann J, Frieler K (2013) Consistent increase in Indian monsoon rainfall and its variability across CMIP-5 models. Earth Syst Dyn 4:287–300

Moss RH, Edmonds JA, Hibbard KA, Manning MR and others (2010) The next generation of scenarios for climate change research and assessment. Nature 463: 747–756

Patton CP (1962) A note on the classification of dry climate in the Köppen system. Calif Geogr 3:105–112

Rogelj J, Meinshausen M, Knutti R (2012) Global warming under old and new scenarios using IPCC climate sensitivity range estimates. Nat Clim Change 2:248–253

Rubel F, Kottek M (2010) Observed and projected climate shifts 1901–2100 depicted by world maps of the Köppen-Geiger climate classification. Meteorol Z 19:135–141

Taylor K, Balaji V, Hankin S, Juckes M, Lawrence B, Pascoe S (2012a) CMIP5 Data Reference Syntax (DRS) and controlled vocabularies. http://pcmdi-cmip.llnl.gov/xmip5/docs/cmip5_data_refernce_syntax.pdf (accessed 7 Nov 2016)

Taylor K, Stouffer RJ, Meehl GA (2012b) An overview of CMIP5 and the experiment design. Bull Am Meteorol Soc 93:485–498

Trewartha GT (1968) An introduction to climate. McGraw-Hill, New York, NY

Trewartha GT, Horn LH (1980) Introduction to climate, 5th edn. McGraw Hill, New York, NY

Willmott CJ, Matsuura K (2001) Terrestrial air temperature and precipitation: monthly and annual time series (1950–1999). http://climate.geog.udel.edu/~climate/html_pages/README.ghcn_ts2.html

Editorial responsibility: Tim Sparks, Cambridge, UK

Submitted: February 22, 2016; Accepted: July 24, 2016
Proofs received from author(s): November 3, 2016